Surface Circular Photogalvanic Effect in Tl-Pb Monolayer Alloys on Si(111) with Giant Rashba Splitting

Ibuki Taniuchi, Ryota Akiyama, Rei Hobara, and Shuji Hasegawa*

Department of Physics, The University of Tokyo, Bunkyo, Tokyo 113-0033, Japan

*akiyama@surface.phys.s.u-tokyo.ac.jp

ABSTRACT

We have found that surface superstructures made of "monolayer alloys" of Tl and Pb on Si(111), having giant Rashba effect, produce non-reciprocal spin-polarized photocurrent via circular photogalvanic effect (CPGE) by obliquely shining circularly polarized near-infrared (IR) light. CPGE is here caused by injection of in-plane spin into spin-split surface-state bands, which is observed only on Tl-Pb alloy layers, but not on single-element Tl nor Pb layers. In the Tl-Pb monolayer alloys, despite of their monatomic thickness, the magnitude of CPGE is comparable or even larger than the cases of many other spin-split thin-film materials. A model analysis has provided the relative permittivity ε^* of the monolayer alloys to be ~ 1.0, which is because the

monolayer exists at a transition region between vacuum and the substrate. The present result opens the possibility that we can optically manipulate spins of electrons even on monolayer materials.

KEYWORDS: Rashba effect, monolayer, surface superstructure, circular photogalvanic effect, spin-polarized current, circular polarized light, spintronics

Spin degree of freedom of electrons is expected to be useful for developing devices for very low energy dissipation and quantum computing. So far, a lot of experiments of spin injection into non-magnetic materials such as semiconductors[1,2], graphene[3,4], and topological insulators[5,6] have been demonstrated using ferromagnetic electrodes and electromagnetic wave application[7,8]. Recently an alternative type of method for spin injection is rising by using spin-angular momentum of light illuminating materials having strong spin-orbit interaction (SOI). SOI lifts spin degeneracy to make voluntarily spin-split bands even for non-magnetic materials, where spin-selective optical excitations can occur with circularly polarized light (CPL) due to the conservation law of angular momentum.

Some papers already report such an optical spin injection into materials, producing spin-polarized electrical current[9,10]. Among them, circular photogalvanic effect (CPGE) attracts much attention because of its simplicity. The spin-selective optical transitions make asymmetric electron excitation in *k*-space, resulting in helicity-dependent photocurrent (HDP) flowing in a particular direction. Such non-reciprocal HDP is spin-polarized because of spin-momentum locking by strong SOI. CPGE is recently reported on many systems such as transition-metal

dichalcogenides[11,12], topological insulators[13-15], and Rashba surface/interface systems[16-18]. In such two-dimensional systems, space inversion symmetry is innately broken down in the plane-normal direction, where spin-split surface bands often appear, and thus it is important to make the excitations at surfaces/interfaces dominate over those in the bulk of the substrate. For this, there are various attempts to control the excitations, such as amplifying optical responses by metamaterials[19] and band tuning with dual gates voltage[20].

In addition, it should be noted that the HDP can be induced not only by CPGE but also by photo-induced inverse spin Hall effect (PISHE)[9]. Therefore, we should be careful in separating the effect incorporated in HDP. Monolayer film systems like in the present study make the interpretation simpler and can be useful for atomic-scale spintronics devices.

It is interesting to explore HDP in monolayer thin-film systems and surface superstructures because the magnitude of Rashba effect sensitively depends on the details of their atomic arrangements and species[21-23]. However, HDP on such monolayers and surface superstructures has not yet been fully studied because it had been naively believed that their thickness is too thin to produce HDP strong enough for detection, and also because *in situ* optical measurements in ultra-high vacuum (UHV) are needed to preserve the well-defined monolayer/surface structures.

In this letter, we report on strong HDP produced by CPGE with spin-selective inter-band excitations in the giant Rashba spin-split surface-state bands of surface superstructures for the first time in monolayer (Tl, Pb) alloys on Si(111) showing ($\sqrt{3} \times \sqrt{3}$) and (4×4) periodicities. We recently reported that the ($\sqrt{3} \times \sqrt{3}$) and (4×4) phases of monolayers have giant Rashba spin-split surface bands (up to an energy splitting ΔE ~ 250 meV) confirmed by angle-resolved photoemission spectroscopy (ARPES), and both show superconductivity at low temperatures by electrical transport measurements[24,25]. As the Si(111) substrate has a band gap of 1.1 eV, HDP

induced by light, of which energy is lower than the band gap, comes from the surface-state bands of ($\sqrt{3} \times \sqrt{3}$) and (4×4) surface superstructures only.

Since the surface Rashba systems show almost in-plane spin polarization, we need to illuminate CPL on the sample surface obliquely to inject the in-plane spin components. By reversing the polarity of CPL or the incident angle of light with respect to the surface-normal direction, the directions of HDP and spin of the flowing electrons are reversed. As a characteristic property of CPGE, when the incident beam of light is perpendicular to the surface, both charge and spin currents do not flow because the incident photons do not have in-plane spin components. In this way, CPGE can be explained by the combination of spin-split bands and selection rules at the optical transition[18].

Methods

To measure the well-defined samples in this study, we fabricated samples by molecular beam epitaxy (MBE) method, combined with *in situ* reflection-high-energy electron diffraction (RHEED) structure analysis in a custom-made UHV chamber, and sequentially measured them electrically *in situ* in the same chamber by illuminating the light without exposing the samples to air, as shown in Fig. 1(a). An example of the RHEED pattern of Si(111)-($\sqrt{3} \times \sqrt{3}$)-(Tl, Pb) is shown in Fig. 1(b). The Si(111) substrate was 3 mm × 10 mm × 0.5 mm in size and *n*-type moderately-doped (the resistivity ρ = 1 - 5 Ω·cm at room temperature). First, Si(111)-(1×1)-Tl was prepared by depositing one monolayer (ML) Tl from a Knudsen cell onto a Si(111)-(7×7) surface held at ~ 300 ℃, where 1 ML = 7.8×10^{14} cm^{-2}, the topmost-layer atom density of Si(111) unreconstructed surface. Then, Pb was deposited from an alumina effusion cell on Si(111)-(1×1)-Tl at room temperature. Depending on the amount of deposited Pb, the surface superstructures of

(Tl, Pb) alloy layer show single phases of ($\sqrt{3} \times \sqrt{3}$) and (4×4) periodicity at Pb coverage of 1/3 ML[25] and 2/3ML[22], respectively. Si(111)-(4×4)-(Tl, Pb) surface superstructure (Fig. 1(c)) was made by adding 1/3ML Pb atoms on Si(111)-($\sqrt{3} \times \sqrt{3}$)-(Tl, Pb) surface (Fig. 1(d)) after the photocurrent measurements for the ($\sqrt{3} \times \sqrt{3}$) surface. For reference, we also made and measured single-component samples covered by 1 ML Tl only (Si(111)-(1×1)-Tl) and covered by 2 ML Pb only (nominal 2-ML-Pb thin film).

The laser beam was chopped by a light chopper, and passed through a lens, a polarizer and a quarter-wave plate (QWP), and finally introduced into the UHV chamber through an optical fused viewport (Fig. 1(a)). The light was generated by CW lasers with the wavelength λ = 635 nm and 1550 nm, and illuminated on the center of the sample with the diameter of the laser spot ~ 1 mm. The power of the IR laser used was 2 mW and the power density was 2.5 mW/cm^2 ,which was confirmed low enough for preventing any heating effects. We monitored the laser intensity with a power meter to estimate the time required for the output to be stabilized sufficiently, and waited at least for that time before starting the measurements. The invisible infrared (IR) laser (λ = 1550 nm) was aligned using the guide of a visible laser (λ = 635 nm) in the setup. The incident angle of RHEED and lasers can be changed between θ = - 60° - + 60° by rotating the sample holder as shown in Figs. 1(a) and (e). The photocurrent induced by the light illumination was measured at room temperature with electrodes clamping the sample at both ends and detected by a lock-in amplifier synchronized with the chopper frequency operated at 196 Hz. The center position was defined as the midpoint of both ends where the photocurrent disappears along both *x*- and *y*-directions (Fig. 1(e)) (see Supplementary Information section S7 and S8 for more detail).

Results

CPGE observation in (Tl, Pb)/Si(111) alloy surface under NIR CPL illumination

Figure 2 shows the light polarization dependence of the photocurrent on Si(111)-($\sqrt{3}\times\sqrt{3}$)-(Tl, Pb) with the laser of wavelength λ = 1550 nm at the angle of incidence θ = - 60° (a), and θ = + 60°(b), respectively (see Supplementary Information section S5 for the data of wavelength λ = 635 nm). The light polarization is changed by rotating the QWP by the angle α; linearly polarized light (α = 0°, 90°, 180°), left-handed CPL (α = 45°), and right-handed CPL (α = 135°). (a) and (b) show changes with the periodicities of 180° (left- and right-handed CPL) as well as 90° (linearly polarized light), with opposite sign of changes between (a) and (b), which directly indicates that the photocurrent induced by the left-handed CPL is different from that by the right-handed CPL in (a) and (b).

Since the photocurrent components contributed by the circularly and linearly polarized light have periodicities of 180° and 90°, respectively, the photocurrent can be expressed phenomenologically as a function of α by[18],

$$J = C \sin 2(\alpha + \alpha_0) + L_1 \sin 4(\alpha + \alpha_0) + L_2 \cos 4(\alpha + \alpha_0) + D. \quad (1)$$

Here, C represents the component in photocurrents due to CPL, that is to say, HDP, while L_1 and L_2 represent the components due to the linearly polarized light, *i.e.*, the linear photogalvanic effect and the linear photon drag effect, respectively. D is the component independent of the light polarization such as the thermoelectric effect and the photovoltaic effect. In the present study, we focus on the first term in Eq. (1) only. A phase shift α_0 is an offset derived from the experimental setup; α_0 = 2.7° and 1.6° for λ = 1550 nm measurements for Si(111)-($\sqrt{3}\times\sqrt{3}$)-(Tl, Pb) and Si(111)-(4×4)-(Tl, Pb), respectively.

To evaluate the relative magnitude of CPGE in the total polarization-dependent components including the L_1 and L_2 terms, the following equation is often used[17,26],

$$\rho_{circ} = \frac{|C|}{|C| + |L_1| + |L_2|}. \quad (2)$$

ρ_{circ} for Si(111)-($\sqrt{3} \times \sqrt{3}$)-(Tl, Pb) is estimated to be 0.03 (λ = 635 nm; Fig. S4(a)) and 0.36 (λ = 1550 nm; Fig. 2(a)). This means that CPGE is negligible with λ = 635 nm while it clearly appears with λ = 1550 nm. This is reasonable because the laser with λ = 635 nm (1.95 eV) excites carriers in the Si substrate over the band gap (1.1 eV) to produce photocurrent in nA range, while the laser with λ = 1550 nm (0.80 eV) cannot excite them in the substrate, resulting in three orders of magnitude smaller photocurrent in pA range, as shown in Fig. 2 and Fig. S4. In other words, the light of λ = 1550 nm is suitable to efficiently detect CPGE from the surface superstructures of (Tl, Pb) alloys only.

CPGE at various angle of incidence of CPL

The flow direction of the photocurrent by CPGE is determined by the crystal symmetry. The surface superstructures of Si(111)-($\sqrt{3} \times \sqrt{3}$)-(Tl, Pb) and (4×4)-(Tl, Pb) have C_{3v} and C_3 symmetry, respectively. In this case, because e_z element in γ-tensor[18] becomes zero (see Supplementary Information), CPGE does not occur with a normal incidence of light, but the oblique incidence of light induces in-plane spin components by CPL, so that CPGE occurs. During CPGE, the electrical current flows perpendicular to the incident plane of light due to the spin-momentum locking effect and the helical spin texture[12,13,25].

When the sample is illuminated by the light at an angle θ in *xz*-plane as shown in Fig. 1(e), the CPGE photocurrent flows along *y*-direction, as described by[18]

$$j_y^{CPGE} = \gamma_{yx} \hat{e}_x(\theta) E_0^2 P_{circ} \propto C(\theta) \quad (3)$$

Here, j is the photocurrent density, γ is a second-rank pseudo-tensor which contains the information of crystal symmetry of the sample and the degree of spin-split e.g. Rashba parameter. $\hat{e}_x$ is the *x*-component of the unit vector including the transmission coefficients and refraction

effect of light, indicating the light propagation in *xz*-plane inside the material, E_0 is the amplitude of the electric field of the incident light, $P_{\mathrm{circ}} = \sin 2(\alpha+\alpha_0)$ is the degree of circular polarization. As described in Supplementary Information note 4, Eq. (3) corresponds to the first term in Eq. (1), and the magnitude of CPGE photocurrent is written by $C(\theta)$ (same as C in Eq. (1)) using Fresnel's transmission coefficient as follow:

$$C(\theta) = A\hat{e}_x(\theta) = A \cdot \frac{4\cos^2\theta \cdot \sin\theta}{\left(\cos\theta + \sqrt{\varepsilon^* - \sin^2\theta}\right)\left(\varepsilon^*\cos\theta + \sqrt{\varepsilon^* - \sin^2\theta}\right)} . \qquad (4)$$

A is the amplitude of CPGE photocurrent (proportional to the light intensity and γ), and ε^* is the relative permittivity of materials causing CPGE. Under the normal incidence of light ($\theta = 0°$), $C(0) = 0$ means that no CPGE occurs. As described in Supplementary note 4 with some discussion supporting the conclusion, since Eq. (4) is based on the Fresnel equations and Snell's law of refraction and transmission of light at the interface between vacuum and material thicker than the light wavelength, there remains room for discussion if this equation is applicable to monatomic-layer systems like in the present study.

The experimental data of C values in Eq. (1) with light of $\lambda = 1550$ nm were taken under different incident angles θ for four samples, Si(111)-($\sqrt{3}\times\sqrt{3}$)-(Tl, Pb), Si(111)-(4×4)-(Tl, Pb), Si(111)-(1×1)-Tl (1 ML), and nominal 2-ML-Pb thin film (2 ML). The results are displayed in Figs. 3 (a) and summarized in Fig.3 (b). The θ dependences of parameter C in each sample were fitted by Eq. (4) as shown in Fig. 3(a) by each curve (Note: we substitute $\theta + \theta_0$ for θ in Eq. (4) for the slight misalignment of the angle as well as the fitting by Eq. (1); the resultant $\theta_0 = -3.0°$). For both (Tl, Pb) alloy surface superstructures, the parameter C is significantly enhanced with increasing θ, whose tendency is consistent with that of CPGE described by Eq. (4). It should be noted here that the possibility of PISHE can be excluded; if PISHE occurs by the surface-normal

component of electron spin which is injected under the normal incident of light, the parameter C does not become negligibly small at $\theta = 0°$. This is not the case in Fig. 3(a). Moreover, as shown in Supplementary Information, the sign of parameter C is not reversed at the opposite edges of sample, which is in contrast to the case of PISHE in Ref. [9].

On the other hand, in cases of single-element metal overlayers, Tl or Pb on Si(111), the parameter C is quite small at all incident angles θ in Fig. 3(a). As shown in Fig. 3 (b) their CPGE amplitudes (parameter A in Eq. (4)) are negligibly small enough to be interpreted as no significant CPGE signal. The reason for this small A can be understood by their band structures and optical excitation processes. The surface bands of Si(111)-(1×1)-Tl have been studied in detail using spin-resolved ARPES and spin- and angle-resolved inverse-photoemission (SRIPE) measurements[27-29]; the energy splitting by the Rashba effect occurs around $\bar{\Gamma}$ point, with the energy splitting $\Delta E \sim 20$ meV and the Rashba parameter $\alpha_R = 0.05$ eV Å[27], which are, however, one order of magnitude smaller than those of (Tl, Pb) alloy surface superstructures ($\alpha_R \sim 0.42$ eV Å for $(\sqrt{3} \times \sqrt{3})$-(Tl, Pb)[25], and $\alpha_R \sim 0.27$ eV Å for (4×4)-(Tl, Pb)[22]). In addition, though Si(111)-(1×1)-Tl has spin-splitting by $\Delta E \sim 0.6$ eV above E_F around $\bar{K}$ point, the spin direction is perpendicular to the surface[28,29]. This is why oblique incidence of light cannot induce the CPGE current. The nominal 2-ML-Pb thin film also shows negligible CPGE due to the small Rashba parameter ($\alpha_R = 0.076$ eV Å[30]) and dense bands crossing the Fermi level E_F[31]; such dense metallic bands around E_F produce photocurrent irrespective of the polarization of light.

Discussion

There are giant Rashba splittings in the metallic surface bands having opposite in-plane spin components on Si(111)-$(\sqrt{3} \times \sqrt{3})$-(Tl,Pb) (the energy splitting $\Delta E_{max} \sim 250$ meV and the band

shift along the wavenumber axis $\Delta k_{max} \sim 0.050$ Å^{-1} [25]) and Si(111)-(4×4)-(Tl, Pb) ($\Delta E_{max} \sim 105$ meV and $\Delta k_{max} \sim 0.047$Å^{-1} [22]) in the vicinity of $\bar{\Gamma}$ point, so that photo-excitations occur between them by oblique illumination of CPL . In Fig. 4, possible photo-excitations are shown in the calculated band dispersions. The red and blue curves in the band dispersions indicate spin-polarized bands due to Rashba splitting by calculation in the previous research[22,23]. The E_F position is revealed by ARPES observations in Si(111)-($\sqrt{3} \times \sqrt{3}$)-(Tl,Pb)[25] and is shown by an orange dotted line in Fig. 4(a), while for Si(111)-(4×4)-(Tl, Pb) the experimental band dispersion and E_F position are still unknown although it is known to be metallic by electrical transport measurements[24]. Some of the possible photo-excitations are shown by arrows, of which length corresponds to the photon energy of ~ 0.8 eV (for $\lambda = 1550$ nm) and of which color gradation means spin-flip excitation by the selection rule. Since the photon energy is larger than energy separations between many pairs of bands for CPGE, various excitation patterns are possible. However, here we have drawn arrows indicating transitions for which a large CPGE signal is expected; they show examples that satisfy the conditions of a larger JDOS, a larger Rashba spin splitting, and less cancellation of spin-dependent excitation.

The first important point is that, unlike a Si substrate, both surface superstructures of Si(111)-($\sqrt{3} \times \sqrt{3}$)-(Tl, Pb) and Si(111)-(4×4)-(Tl, Pb) become direct transition type with the emergence of new surface bands due to band-folding by superstructure and splitting by Rashba spin-orbit coupling. Therefore, a myriad of critical points having large joint density-of-states (JDOS) related to optical absorption appear. In the case of Si(111)-($\sqrt{3} \times \sqrt{3}$)-(Tl, Pb), critical points can be $\bar{M}$, $\bar{\Gamma}$, $\bar{K}$ and the branches stretch between them as shown in Fig. S5(a) in Supplementary Information, but we can exclude $\bar{\Gamma}$ point because the photon energy is lower than the energy gap at $\bar{\Gamma}$ point. On

the other hand, in the case of Si(111)-(4×4)-(Tl, Pb), there are many critical points other than $\bar{M}$, $\bar{\Gamma}$, and $\bar{K}$ as shown in Fig. S5(b) in Supplementary Information, so we cannot narrow down the excitation paths. In the case of very simplified band structures, the larger Rashba parameter is, the larger CPGE amplitude (parameter *A*) is usually expected, because the CPGE current includes contributions proportional to Rashba and Dresselhaus parameters [32]. However, the CPGE amplitude *A* does not differ so much between $(\sqrt{3}\times\sqrt{3})$-(Tl, Pb) and (4×4)-(Tl, Pb) as shown in Fig. 3(b) although their Rashba parameters are quite different from each other ($\alpha_R \sim 0.42$ and ~ 0.27 eV Å for the respective surfaces[25, 22]). This may be because the 4×4-(Tl, Pb) surface has much more dense bands than $(\sqrt{3}\times\sqrt{3})$-(Tl, Pb) as shown in Fig. 4(b) and Fig. S5, so that much more photo-excitations are possible which in turn may reduce the asymmetric degree of photoexcitation in *k*-space with respect to high symmetry points. Therefore, the magnitude of the Rashba parameter is important, but not the only dominant factor in deciding the magnitude of CPGE. The CPGE amplitude is also affected by the JDOS of the bands regarding excitations, as well as how crowded and asymmetric the spin-splitting bands are (the degree to which the induced photocurrent survives by avoiding canceling out with opposite photocurrent).

The optical response of monolayer features has not been investigated enough; only a few examples have been reported where the authors claim that the signal comes from the thin surface layers only though their samples are as thick as bulk crystals[11,12]. Especially the refraction of light has not been discussed for monolayer materials. Intriguingly, thanks to *in situ* measurements in our UHV systems in which we do not need any capping layer on the sample surface for protection, we have found that, from the fitting by Eq. (4), the relative permittivity ε^* is almost unity for the (Tl, Pb) alloy layers (the values are shown in Fig. 3(b)). This means that, though the absorption of photons occurs at the monolayer enough to produce the HDP, the layer is extremely thin and

located in a transition region between vacuum and the substrate, preventing from differentiating the relative permittivity from that of vacuum. In other words, it supports that CPGE surely comes from the surface bands of the monolayers. In previous reports *e.g.*, topological insulators and Rashba interface systems[17,33], ε^* is significantly larger than unity because of the capping layer and/or the large thickness of the samples; the refraction and transmission of light occurs at the absorptions of photons inside the materials. See Supplementary Information for the detailed discussion.

In the fitting results of A and ε^* by Eq. (4) for 1 ML Si(111)-(1×1)-Tl and nominal 2-ML-Pb thin films, the amplitude A of CPGE is quite small, which brings us to the relatively large indefiniteness of ε^*. This is reflected in the error bars for ε^* of 1 ML Si(111)-(1×1)-Tl and nominal 2-ML-Pb thin film in Fig. 3(b); it is difficult to have definite discussion about the dielectric constants in these two cases beyond the margin of error. On the other hand, for samples having the large amplitude A of CPGE, Si(111)-($\sqrt{3} \times \sqrt{3}$)-(Tl, Pb) and Si(111)-(4 × 4)-(Tl, Pb), it is possible to have definite discussion about ε^* values because the fitting results by Eq. (4) keep the relative error of ε^* small enough.

In Fig. 5, let us compare our work with other reported systems in terms of the "background" band gap (ordinate), the sample thickness (abscissa), and the amplitude of CPGE ρ_{circ} (point diameter) defined by Eq. (2). Here, the "background" band gap is defined as the bandgap inducing excitations that screen out the electrical current of CPGE. Namely, in our system, the background bandgap is that of the Si substrate. In such meaning, material systems with large background gaps are more suitable for CPGE observation. As seen in Fig. 5, first, whereas our samples are the thinnest among them, the CPGE amplitude is comparable to or relatively higher than the listed cases[11,13-16,19,26]. This benefits the atomic-layer opto-spintronics devices. Second, our monolayer

samples are on the substrate having the largest band gap among listed cases, which prevents other undesired optical excitations. Although the surface superstructure is very thin so that the absorption of light had been considered too small to induce significant spin-dependent optical phenomena, we have succeeded here in showing significant CPGE.

In summary, contrary to the naive conviction, we have observed strong CPGE producing non-reciprocal photocurrent on the monolayer surface superstructures, Si(111)-($\sqrt{3} \times \sqrt{3}$)-(Tl, Pb) and (4×4)-(Tl, Pb), for the first time. This is due to spin injection to excite electrons between Rashba-type spin-split surface bands. In addition, the relative permittivity ε^* of the monolayers is estimated to be ~ 1 from the light incident-angle dependence of CPGE. This is natural by considering that the surface superstructures are only single-atom thick and located in a transition region between vacuum and the substrate. In other words, this strongly indicates that the CPGE observed here is derived from surface superstructures. These results show an impactful fact to the field that structures with only one atomic layer can excite significant spin-polarized current due to spin-momentum locking as a result of Rashba spin split surface bands at room temperature by irradiating circular polarized light, which can then be detected electrically, and pave the way to "surface opto-spintronics.

FIGURES

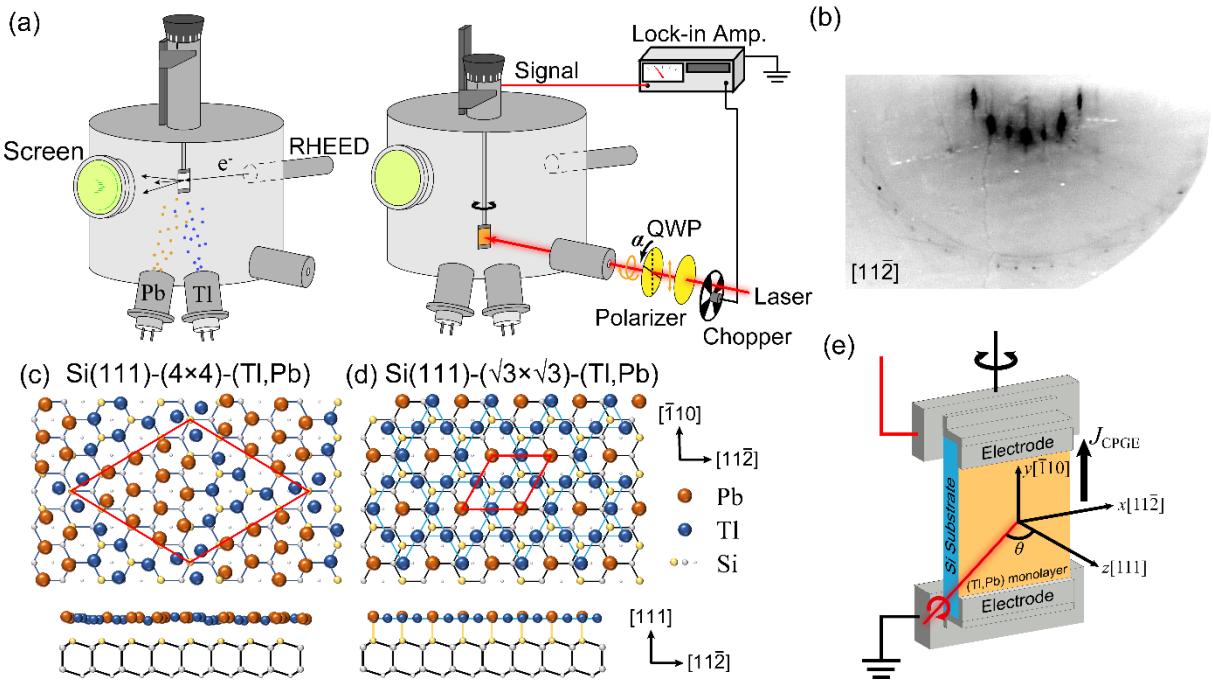

Fig. 1| experimental setup and overview of (Tl, Pb)/Si(111). a Schematics of the experimental set-up during the sample growth (left) and the optical measurements (right) in the UHV chamber. **b** RHEED pattern with the incident electron beam of [11$\bar{2}$] of the Si(111) substrate just after the growth of the (√3×√3)-(Tl,Pb) monolayer on Si(111). (c,d) Top view and cross-sectional view of the atomic structures of **c** Si(111)-(4×4)-(Tl, Pb) and **d** Si(111)-(√3×√3)-(Tl, Pb) surface superstructures[22,25]. **e** Detailed figure around the sample. The photocurrent is generated by irradiating the laser on, and is detected by metal (Mo) electrodes clamping both ends of the sample. The sample can be rotated to change the angle of incidence of the laser beam.

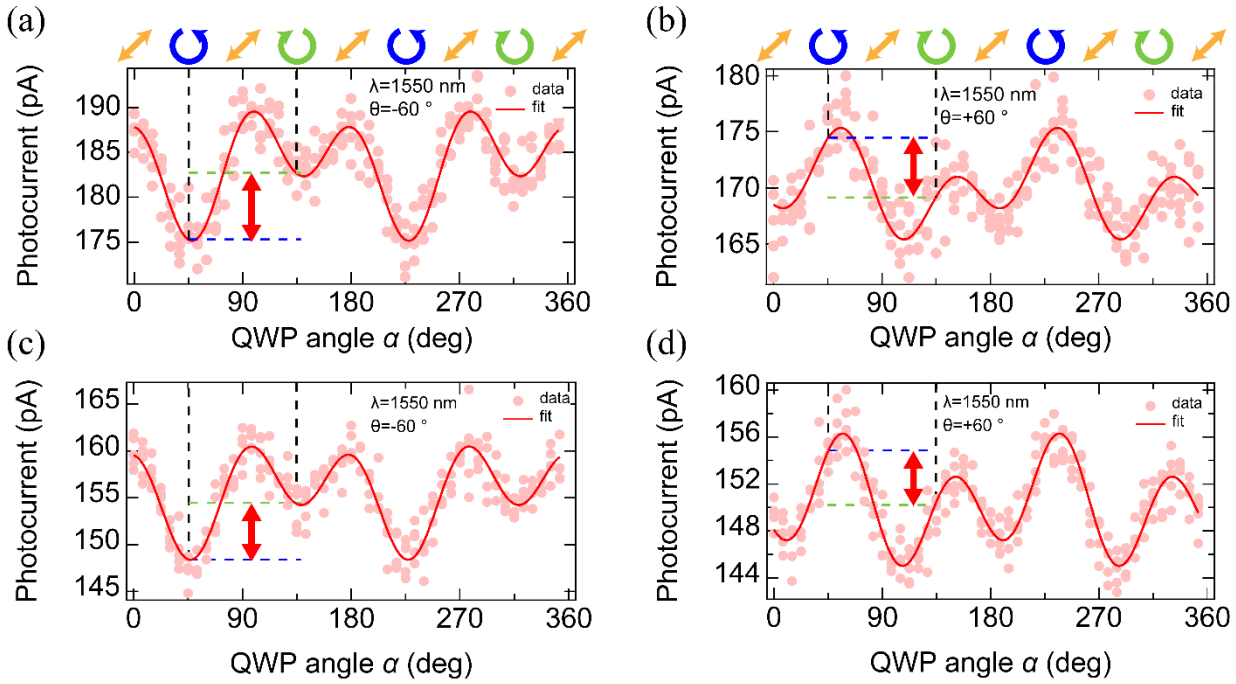

Fig. 2| Polarization dependence of the photocurrent measured on a, b Si(111)-($\sqrt{3}\times\sqrt{3}$)-(Tl, Pb) and c, d Si(111)-(4 × 4)-(Tl, Pb) with λ = 1550 nm, at the angle of light incidence **a, c** θ = - 60° and **b, d** θ = + 60°, respectively. The light is polarized by rotating the QWP with angle α, and the polarization is shown at the top of each graph. Scans for five times represented by light colored dots are plotted, and deep-colored solid curves are the fitting results by Eq. (1). The green (blue) dashed line indicates the photocurrent value for the right-handed (left-handed) CPL. The difference between the two dashed lines indicated by red arrow corresponds to HDP, which is twice as much as the parameter C in Eq. (1).

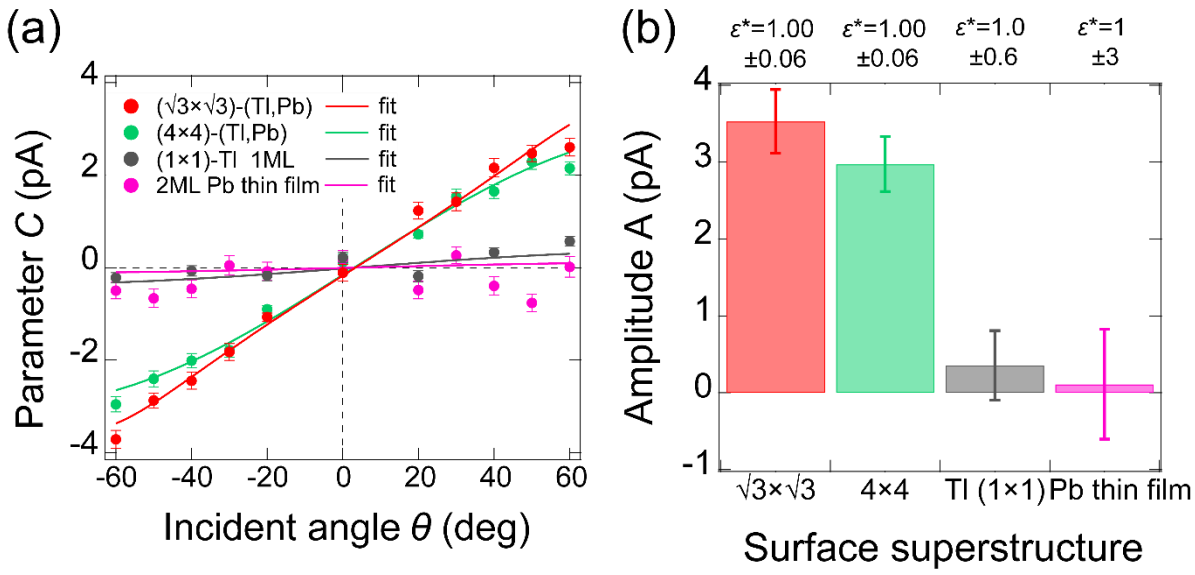

Fig. 3| enhancement of CPGE under oblique incidence of CPL. **a** Light incident angle θ dependence of parameter C in Si(111)-($\sqrt{3}\times\sqrt{3}$)-(Tl, Pb), Si(111)-(4×4)-(Tl, Pb), Si(111)-(1×1)-Tl, and nominal 2-ML-Pb thin film. The parameter C was obtained by fitting the α dependence of the photocurrent using Eq. (1) at each incident angle θ. Solid lines are fitting curves by Eq. (4) for the respective surfaces. **b** CPGE amplitude A in Eq. (4) of each sample. Si(111)-($\sqrt{3}\times\sqrt{3}$)-(Tl, Pb) and Si(111)-(4×4)-(Tl, Pb) show significantly larger amplitudes than Si(111)-(1×1)-Tl and nominal 2-ML-Pb thin film which show negligibly small CPGE. The fitting results of relative permittivity ε^* are shown on top of each bar chart.

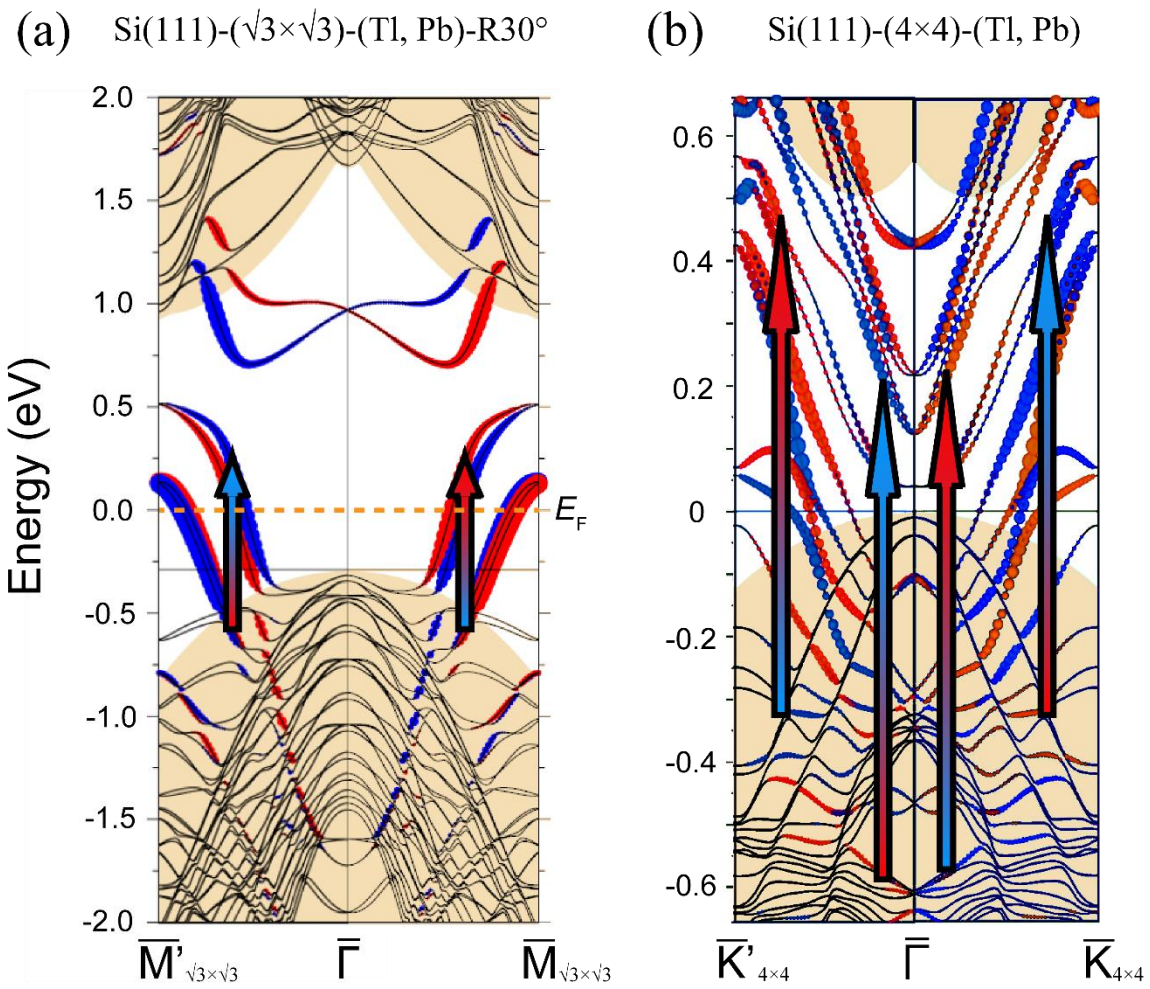

Fig. 4| band dispersion of (Tl, Pb)/Si(111) surface state and possible excitation paths. The calculated band structures of **a** Si(111)-($\sqrt{3}\times\sqrt{3}$)-(Tl, Pb), where orange dotted line indicates the Fermi level determined by experiments, and **b** Si(111)-(4×4)-(Tl, Pb)[22,23]. Red and blue colors represent the surface Rashba split bands. The depicted arrows having length of 0.8 eV indicate possible representative optical excitation paths, and the gradient color in arrows mean the spin-flip excitation by the selection rule. **a** is reprinted and modified from Ref. [23], Copyright (2017), with permission from American Physical Society. **b** is reprinted and modified from Ref. [22], Copyright (2017), with permission from Elsevier.

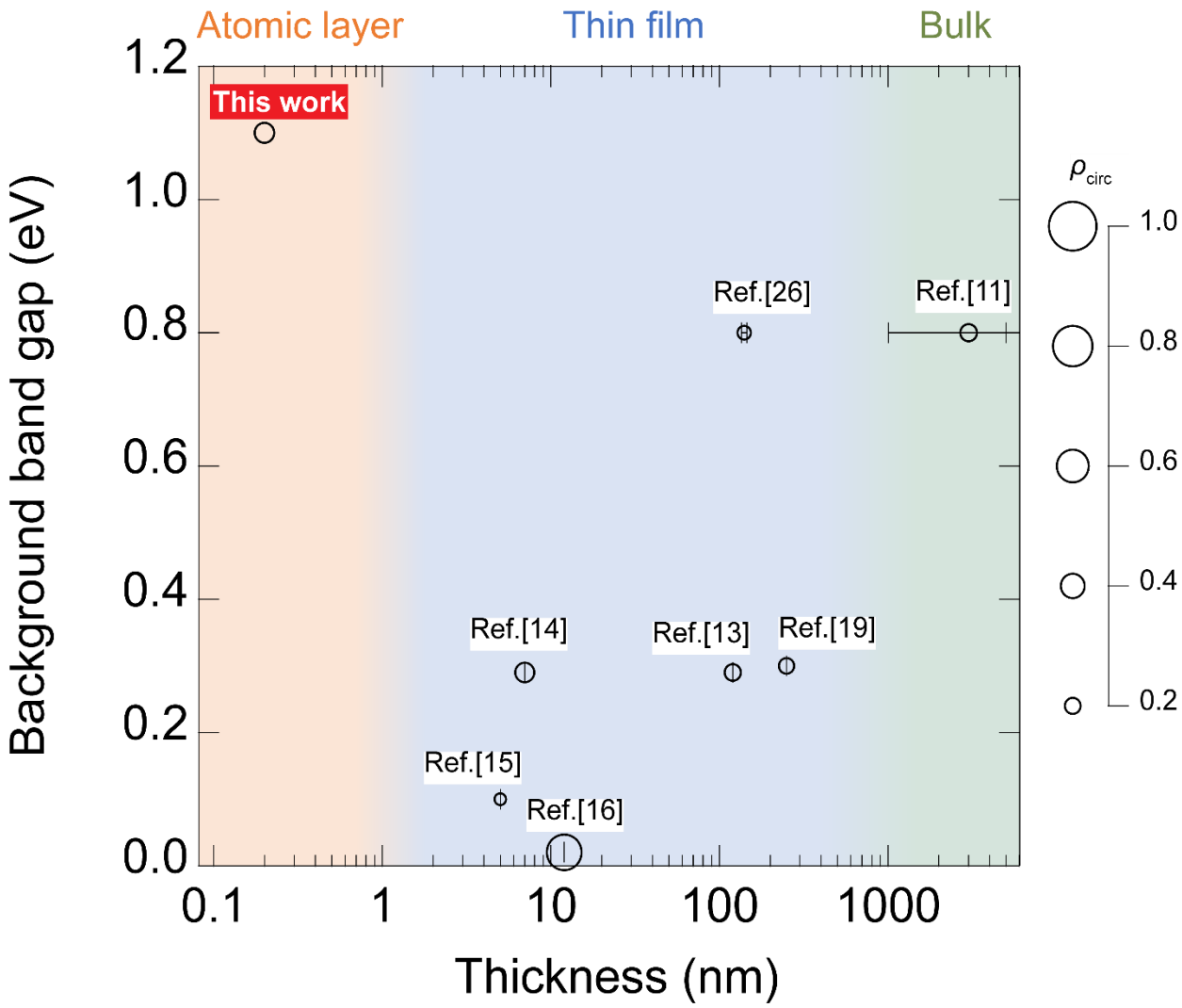

Fig. 5| Comparison of CPGE reported in various systems. The diameter of each marker represents the CPGE amplitude ρ_{circ} defined by Eq. (2). For the thicknesses of materials under measurements, we have adopted the values available in the literature. When the values are not available, we have estimated them with error bars. For the background band gap, which is defined as the bandgap inducing excitations that screen out the electrical current of CPGE. Smaller values are adopted when those of substrate and films are different in order to compare the ease of access to spin-split surface band dispersions which appear within the background band gap. The background color depicts a rough classification of samples in terms of thickness into atomic layers

(orange), thin films (sky blue), and bulk materials (light green). In the case that CPGE is enhanced by some operation such as gate tuning or optical resonance, ρ_{circ} is determined in the bare state.

ASSOCIATED CONTENT

Supporting Information

The Supporting Information is available free of charge.

AUTHOR INFORMATION

Corresponding Author

*E-mail: akiyama@surface.phys.s.u-tokyo.ac.jp.

Author Contributions

IT fabricated samples with help of RA. IT planned and performed set-up of the apparatus and optoelectrical measurements with advised by RA, RH, and SH. RA conceive and design experiments. All authors take part in discussing experimental results and interpretation. IT, RA, and SH wrote the manuscript with contributions from all the authors. SH supervised the whole project.

Funding

This research was partly supported by JSPS KAKENHI Grant Nos. 20H00342, 20H02616, and 22K18934.

Notes

The authors declare no competing financial interest.

ACKNOWLEDGMENTS

We thank Dimitry Gruznev and Alexander A. Saranin in Institute of Automation and Control Processes for their advice to make better samples. We also thank Shunsuke Sato for his help in discussion and diagramming. I.T. is supported by JSPS Research Fellowships for Young Scientists and the WINGS-QSTEP program of the University of Tokyo.

References

1. Ohno, Y., Young, D. K., Beschoten, B., Matsukura, F., Ohno, H. & Awschalom, D. D. Electrical spin injection in a ferromagnetic semiconductor heterostructure. Nature (London) **402**, 790–792 (1999).

2. Hammar, P. R., Bennett, B. R., Yang, M. J. & Johnson, M. Observation of Spin Injection at a Ferromagnet-Semiconductor Interface. Phys. Rev. Lett. **83**, 203 (1999).

3. Yamaguchi, T., Inoue, Y., Masubuchi, S., Morikawa, S., Onuki, M., Watanabe, K., Taniguchi, T., Moriya, R. & Machida, T. Electrical Spin Injection into Graphene through Monolayer Hexagonal Boron Nitride. Appl. Phys. Express **6**, 073001 (2013).

4. Ghiasi, T. S., Kaverzin, A. A., Dismukes, A. H., de Wal, D. K., Roy, X. & van Wees, B. J., Electrical and thermal generation of spin currents by magnetic bilayer graphene. Nat. Nanotech. **16**, 788–794 (2021).

5. Shiomi, Y., Nomura, K., Kajiwara, Y., Eto, K., Novak, M., Segawa, K., Ando, Y. & Saitoh, E. Spin-Electricity Conversion Induced by Spin Injection into Topological Insulators. Phys. Rev. Lett. **113**, 196601 (2014).

6. Jamali, M., Lee, J. S., Jeong, J. S., Mahfouzi, F., Lv, Y., Zhao, Z., Nikolic, B. K., Mkhoyan, K. A., Samarth, N. & Wang, JP. Giant Spin Pumping and Inverse Spin Hall Effect in the Presence of Surface and Bulk Spin−Orbit Coupling of Topological Insulator Bi_2Se_3. Nano Lett. **15**, 10, 7126–7132 (2015).

7. Shiomi, Y., Yamamoto, K. T., Nakanishi, R., Nakamura, T., Ichinokura, S., Akiyama, R.,

Hasegawa, S. & Saitoh, E. Efficient Edelstein effects in one-atom-layer Tl-Pb compound. Appl. Phys. Lett. **113**, 052401 (2018).

8. Goel, S., Khang, N. H. D., Osada, Y., Anh, L. D., Hai, P. N. & Tanaka, M. Room-temperature spin injection from a ferromagnetic semiconductor. Sci. Rep. **13**, 2181 (2023)

9. Fan, D., Hobara, R., Akiyama, R. & Hasegawa, S. Inverse spin Hall effect induced by asymmetric illumination of light in topological insulator Bi_2Se_3. Phys. Rev. Research **2**, 023055 (2020).

10. Puebla, J., Auvray, F., Yamaguchi, N., Xu, M., Bisri, S. Z., Iwasa, Y., Ishii, F. & Otani, Y. Photoinduced Rashba Spin-to-Charge Conversion via an Interfacial Unoccupied State. Phys. Rev. Lett. **122**, 256401 (2019).

11. Yuan, H., Wang, X., Lian, B., Zhang, H., Fang, X., Shen, B., Xu, G., Xu, Y., Zhang, SC., Hwang, HY. & Cui, Y. Generation and electric control of spin–valley-coupled circular photogalvanic current in WSe_2. Nat. Nanotech. **9**, 851–857 (2014).

12. Quereda, J., Ghiasi, T. S., You, JS., van den Brink, J., van Wees, B. J. & van der Wal, Caspar H. Symmetry regimes for circular photocurrents in monolayer $MoSe_2$. Nat. Commun. **9**, 3346 (2018).

13. McIver, J. W., Hsieh, D., Steinberg, H., Jarillo-Herrero, P. & Gedik, N. Control over topological insulator photocurrents with light polarization. Nat. Nanotech. **7**, 96–100 (2012).

14. Zhuang, H., Yu, J., Chen, L., Gu, P., Chen, Y., Liu, Y., Yin, C., Lai, Y. & Cheng, S. J. Giant circular photogalvanic effect of the surface states in an ultra-thin Bi_2Se_3 nanoplate grown by chemical vapor deposition. Appl. Phys. **129**, 105303 (2021).

15. Yu, J., Xia, L., Zhu, K., Pan, Q., Zeng, X., Chen, Y., Liu, Y., Yin, C., Cheng, S., Lai, Y., He, K. & Xue, Q. Control of Circular Photogalvanic Effect of Surface States in the Topological Insulator Bi_2Te_3 via Spin Injection. ACS Appl. Mater. Interfaces **12**(15), 18091–18100 (2020).

16. Hirose, H., Ito, N., Kawaguchi, M., Lau, YC. & Hayashi, M. Circular photogalvanic effect in Cu/Bi bilayers. Appl. Phys. Lett. **113**, 222404 (2018).

17. Cho, K. S., Liang, C.-T., Chen, Y. F., Tang, Y. Q. & Shen, B. Spin-dependent photocurrent induced by Rashba-type spin splitting in $Al_{0.25}Ga_{0.75}N$/GaN heterostructures。 Phys. Rev. B **75**, 085327 (2007).

18. Ganichev, S. D. & Prettl, W. Spin photocurrents in quantum wells. J. Phys. Condens. Matter **15**, R935–R983 (2003).

19. Sun, X., Adamo, G., Eginligil, M., Krishnamoorthy, H. N. S., Zheludev, N. I. & Soci, C. Topological insulator metamaterial with giant circular photogalvanic effect. Sci. Adv. **7** 14 (2021).

20. Xu, SY., Ma, Q., Shen, H., Fatemi, V., Wu, S., Chang, TR., Chang, G., Valdivia, A. M. M., Chan, CK., Gibson, Q. D., Zhou, J., Liu, Z., Watanabe, K., Taniguchi, T., Lin, H., Cava, V, Fu, V, Gedik, N. & Jarillo-Herrero, P. Electrically switchable Berry curvature dipole in the monolayer topological insulator WTe_2. Nat. Phys. **14**, 900–906 (2018).

21. Bihlmayer, G., Blügel, S. & Chulkov, E. V. Enhanced Rashba spin-orbit splitting in Bi/Ag(111) and Pb/Ag(111) surface alloys from first principles. Phys. Rev. B **75**, 195414 (2007).

22. Mihalyuk, A.N., Hsing, C.R., Wei, C.M., Gruznev, D.V., Bondarenko, L.V., Tupchaya, L.V., Zotov, A.V. & Saranin, A.A. One-atom-layer 4×4 compound in (Tl, Pb)/Si(111) system. Surf.

Sci. **657**, 63-68, (2017).

23. Matetskiy, A. V., Kibirev, I. A., Mihalyuk, A. N., Eremeev, S. V., Gruznev, D. V., Bondarenko, L. V., Tupchaya, A. Y., Zotov, A. V. & Saranin, A. A. Theory versus experiment for a family of single-layer compounds with a similar atomic arrangement: (Tl,*X*)/Si(111) $\sqrt{3}\times\sqrt{3}$(*X*=Pb,Sn,Bi,Sb,Te,Se). Phys. Rev. B **96**, 085409 (2017).

24. Nakamura, T., Takayama, A., Hobara, R., Gruznev, D.V., Zotov, A.V., Saranin, A.A. & Hasegawa, S. Superconducting single-atomic-layer Tl-Pb compounds on Ge(111) and Si (111) surface. Appl. Surf. Sci., **479**, 679-684 (2019).

25. Matetskiy, A. V., Ichinokura, S., Bondarenko, L. V., Tupchaya, A. Y., Gruznev, D. V., Zotov, A. V., Saranin, A. A., Hobara, R., Takayama, A. & Hasegawa, S. Two-Dimensional Superconductor with a Giant Rashba Effect: One-Atom-Layer Tl-Pb Compound on Si(111). Phys. Rev. Lett. **115**, 147003 (2015).

26. Cha, S., Noh, M., Kim, J. Son, J., Bae, H., Lee, D., Kim, H., Lee, J., Shin, HS., Sim, S., Yang, S., Lee, S., Shim, W., Lee, CH., Jo, MH., Kim, J. S., Kim, D. & Choi, H. Generation, transport and detection of valley-locked spin photocurrent in WSe_2–graphene–Bi_2Se_3 heterostructures. Nat. Nanotech. **13**, 910–914 (2018).

27. Sakamoto, K., Oda, T., Kimura, A., Miyamoto, K., Tsujikawa, M., Imai, A., Ueno, N., Namatame, H., Taniguchi, M., Eriksson, P. E. J. & Uhrberg, R. I. G. Abrupt Rotation of the Rashba Spin to the Direction Perpendicular to the Surface. Phys. Rev. Lett. **102**, 096805 (2009).

28. Sakamoto, K., Kim, TH., Kuzumaki, T., Müller, B., Yamamoto, Y., Ohtaka, M., Osiecki, J. R., Miyamoto, K., Takeichi, Y., Harasawa, A., Stolwijk, S. D., Schmidt, A. B., Fujii, J., Uhrberg,

R. I. G., Donath, M., Yeom, H. W. & Oda, T. Valley spin polarization by using the extraordinary Rashba effect on silicon. Nat. Commun **4**,2073 (2013).

29. Stolwijk, S. D., Schmidt, A. B., Sakamoto, K., Krüger, P. & Donath, M. Valley spin polarization of Tl/Si(111). Phys. Rev. Mater. **1**, 064604 (2017).

30. Slomski, B., Landolt, G., Meier, F., Patthey, L., Bihlmayer, G., Osterwalder, J. & Dil, J. H. Manipulating the Rashba-type spin splitting and spin texture of Pb quantum well states. Phys. Rev. B **84**, 193406 (2011).

31. Miyata, N., Horikoshi, K., Hirahara, T., Hasegawa, S., Wei, C. M. & Matsuda, I. Electronic transport properties of quantum-well states in ultrathin Pb (111) films. Phys. Rev. B **78**, 245405 (2008).

32. Giglberger, S., Golub, L. E., Bel'kov, V. V., Danilov, S. N., Schuh, D., Gerl, C., Rohlfing, F., Stahl, J., Wegscheider, W., Weiss, D., Prettl, W. & Ganichev, S. D. Rashba and Dresselhaus spin splittings in semiconductor quantum wells measured by spin photocurrents. Phys. Rev. B **75**, 035327 (2007).

33. Okada, K. N., Ogawa, N., Yoshimi, R., Tsukazaki, A., Takahashi, K. S., Kawasaki, M. & Tokura, Y. Enhanced photogalvanic current in topological insulators via Fermi energy tuning. Phys. Rev. B **93**, 081403(R) (2016).